

Complementary Polarization-Diversity Coherent Receiver for Self-Coherent Homodyne Detection With Rapid Polarization Tracking

Honglin Ji ¹, Jingchi Li ², Xingfeng Li, Shuangyu Dong ¹, Zhaopeng Xu ¹, Yikai Su ¹, *Senior Member, IEEE*, and William Shieh ¹, *Fellow, IEEE*

Abstract—There has been renewed interest in coherent detection to provide high spectral efficiency transmission for short-reach optical interconnects. However, the expensive high-stable laser sources may preclude its potential application. To balance the high performance and low cost for short-reach optical networks, the self-coherent homodyne receiver has been investigated, where the dual-polarization (DP) signal and the remote local oscillator (LO) originating from the same laser source co-propagate over a duplex fiber, enabling a remarkable tolerance of laser linewidth. However, the fast evolution of the state of polarization (SOP) of remotely delivered LO becomes problematic for self-coherent homodyne detection systems. To combat the polarization wandering of the remote LO, the complicated adaptive/automatic polarization controller (APC) has been deployed with only up to a few hundred rad/s polarization tracking speed. In this paper, we propose a complementary polarization-diversity coherent receiver (C-PDCR) for self-coherent homodyne detection using remote LO. The proposed C-PDCR features rapid polarization tracking for remote LO utilizing electronic digital signal processing (DSP). The robustness of the proposed C-PDCR is verified and demonstrated with a 1.08-Tb/s line rate (net rate 769.4 Gb/s over 45-GHz electrical bandwidth) using DP PCS-256QAM signal under rapid polarization rotation rate up to 314 krad/s in the experiment, which is more than 3-orders improvement of magnitude compared to the prior reports.

Index Terms—Coherent detection, polarization multiplexing, remote local oscillator, self-coherent homodyne detection, short-reach optical interconnects.

Manuscript received October 11, 2021; revised December 2, 2021 and January 13, 2022; accepted January 18, 2022. Date of publication January 25, 2022; date of current version May 2, 2022. This work was supported in part by the Australian Research Council (ARC) under Discovery Grants DP150101864 and DP190103724, in part by the National Key Research and Development Program of China under Grant 2019YFB1803602, and in part by the National Natural Science Foundation of China under Grants 61835008 and 61860206001. (Corresponding author: Honglin Ji.)

Honglin Ji, Shuangyu Dong, Zhaopeng Xu, and William Shieh are with the Department of Electrical and Electronic Engineering, The University of Melbourne, Melbourne, VIC 3010, Australia (e-mail: honglinj@student.unimelb.edu.au; shuangyud@student.unimelb.edu.au; zhaopeng@student.unimelb.edu.au; shiehw@unimelb.edu.au).

Jingchi Li, Xingfeng Li, and Yikai Su are with the State Key Laboratory of Advanced Optical Communication Systems and Networks, Department of Electronic Engineering, Shanghai Jiao Tong University, Shanghai 200240, China (e-mail: Jingchi_Lee@sjtu.edu.cn; xingfengli@sjtu.edu.cn; yikaisu@sjtu.edu.cn).

Color versions of one or more figures in this article are available at <https://doi.org/10.1109/JLT.2022.3144983>.

Digital Object Identifier 10.1109/JLT.2022.3144983

I. INTRODUCTION

SHORT-REACH optical networks are commonly cost-sensitive while their capacity requirements have been steadily increasing [1]. Most popular Internet applications, such as cloud computing, mobile video streaming services, and the Internet of Things (IoT), contribute to a major portion of the traffic growth in short-reach optical interconnects. This rapid growth in traffic demand for short-reach optical interconnects necessitates high-speed transmission links and networks. Therefore, 800-Gb/s and 1.6-Tb/s switch interface speeds are envisioned to be the next target in the Ethernet roadmap [2]. To fulfill such data rate requirements, there are normally three design dimensions in optical communications: 1) high-order modulation formats, 2) higher symbol rate per lane, 3) more parallel lanes in polarization, space, and wavelength domain [3]. Therefore, multi-channel parallel optics based on intensity modulation and direct detection (IMDD) are still preferred nowadays for short-reach applications [4]. However, multi-channel parallel optics require many tunable lasers and inefficient modulation formats such as PAM-4 are normally deployed in IMDD based transmission systems. Limited by the required number of wavelengths and component bandwidth, IMDD based parallel transmission systems are hard to scale with the rapid capacity increase. Moreover, the dense wavelength division multiplexing (DWDM) based IMDD systems as a means of multi-channel parallel optics normally employ many un-cooled laser sources, which have large wavelength drift along with the time and should be well managed to cooperate with the receiver-side static wavelength demultiplexing [5]. Thus, DWDM based IMDD systems within a single fiber are much less desired as it significantly increases the operational cost [6].

The difficulty of further scaling up of multi-channel parallel optics reinforces the importance of introducing high-order modulation formats to achieve high spectral efficiency within the allowed channel bandwidth. Multi-level signaling in the Stokes space can further increase the modulation degree of freedom to three but requires double bandwidth for the reception of Stokes parameters [7]–[8]. Therefore, there has been renewed interest in spectrally efficient coherent transmission systems to minimize the amount of parallel hardware and realize the future 800G/1.6T Ethernet speed targets. Conventional coherent detection systems could not only increase the spectral efficiency

by giving access to all the four dimensions of an optical carrier but also provide higher receiver sensitivity than IMDD based transmission systems by mixing the received weak signals with the strong LO. Therefore, coherent detection has enjoyed resounding success in long- or medium-reaches optical transport networks. As aforementioned, in short-reach optical networks, it is cost-sensitive and the dominant cost is in the transceivers. The coherent transceivers consist of narrow-linewidth laser sources, advanced field modulators, coherent receiver front-end, and digital signal processors. Although the cost and footprint of a large portion of the coherent transceivers have been tackled by the optical and electrical integration [9]–[10], the classical coherent detection systems are yet perceived as too costly and power-consuming for short-reach optical interconnects due to the need for expensive high-stable lasers. Most recently, as a compromising solution, polarization-diversity coherent receiver (PDCR) using remote LO has been investigated to both improve the capacity scalability and maintain the low cost for short-reach applications. In such a system configuration, the self-coherent LO originating from the same laser source for DP modulation is remotely delivered to the coherent receiver front-end over a duplex fiber, enabling a remarkable tolerance of laser linewidth [11]. Furthermore, the sophisticated wavelength alignment between the transmitter and receiver is avoided, which allows an un-cooled optical transceiver. Lastly, the carrier/phase recovery algorithms will be greatly simplified in self-coherent homodyne detection systems, which becomes comparable to the DSP used in IMDD systems.

However, the fast evolution of the SOP of remotely delivered LO becomes problematic for self-coherent homodyne detection systems. The so-called polarization fading occurs when the polarization of the received LO is accidentally aligned with one of the local polarizations of the polarization beam splitter (PBS), resulting in the complete loss of the power in the other polarization. To address the inevitable occurrences of the arbitrarily varying SOP and polarization fading of the received remote LO, the APC is generally needed for remote LO in the conventional self-coherent homodyne detection systems to guarantee the strong tone signal beating on both polarizations at the coherent receiver. The APC could transform the excursions of the incoming SOP to the desired output SOP. This transformation must be accomplished in a continuous or an endless manner referred to as reset-free so that the arbitrarily varying SOP can be accommodated without causing abrupt perturbation on the output SOP [12]. Nevertheless, to achieve the transparent polarization transformation, the reset-free APC generally requires complicated device design and algorithm control. Most importantly, the APC must respond to hundreds of krad/s speeds to cope with the fast SOP changes under some extreme conditions such as mechanical vibrations and lightning strikes on cables [13]–[14]. Up until now, the polarization tracking speed of the engineered APC using thermal phase shifters can be only up to a few hundred rad/s [15] without performance degradation, which may not be sufficient for the links that undergo fast mechanical disturbances. Considering the device complexity and currently limited SOP tracking speed of the APC, we have proposed a hybrid Stokes vector receiver and single-polarization coherent

receiver served as a hybrid PDCR (H-PDCR) scheme without requiring optical polarization control for the remotely delivered LO [16]. However, this approach uses a polarization diversity 90-degree optical hybrid, which may be difficult to implement in silicon photonics integration.

In this paper, we further propose a complementary PDCR (C-PDCR) by introducing the third complementary coherent receiver for the remix of LO and signal. In addition to the two 90-degree optical hybrids in the conventional PDCR, the third complementary coherent receiver provides complementary-polarization diversity (CPD) to combat the polarization fading issue of remote LO. To cope with the fast evolution of the unpredictable SOP of remote LO, the polarization tracking algorithm is only based on electronic DSP. The proposed C-PDCR with full 4-D detection is distinguished from other Stokes vector-based receivers such as Stokes vector direct detection (SVDD) receiver and H-PDCR. To demonstrate the robustness of the proposed C-PDCR, a 90-Gbaud DP probabilistic constellation shaped (PCS) 256-QAM signals with 1.08-Tb/s raw data rate is successfully recovered under rapid polarization rotation rate up to 314 krad/s, which features more than 1047-fold polarization tracking speed improvement without performance degradation when compared with the prior reports [15]. In this work, we present more details to our previous publication [17] and provide further characterization of the proposed C-PDCR including the generalized mutual information (GMI) performance, frequency-resolved SNR spectrum, and LO to signal power ratio (LOSPR) dependence.

The paper is organized as follows: Section II elucidates the principle of the proposed C-PDCR. Section III conducts the experiments for the proposed C-PDCR. Section IV presents the experimental results. Section V concludes the paper.

II. PRINCIPLE OF THE PROPOSED C-PDCR SCHEME

To combat the random SOP rotation of the remotely delivered LO for self-coherent homodyne detection, the conventional PDCR involving the APC has been widely investigated. The receiver configuration of the conventional PDCR is shown in Fig. 1(a). To achieve the polarization-diversity reception, two 90-degree optical hybrids are utilized. An incoming random SOP of the remote LO after the polarization splitter/rotator (PSR) is processed by the complicated APC to provide equal carrier power for DP signal coherent detection. Distinguished from the conventional PDCR scheme, we propose a C-PDCR without any optical polarization control, namely APC, for the remote LO, which is illustrated in Fig. 1(b). In addition to the two 90-degree optical hybrids (top and bottom ones), the third 90-degree optical hybrid (middle one) is incorporated in our proposed C-PDCR to achieve complementary polarization detection. In the perspective of hardware complexity, our proposed C-PDCR comprises one more 90-degree optical hybrid followed by two balanced photodetectors (BPDs). However, it is anticipated that the transceiver cost difference between the two PDCR schemes as presented in Fig. 1 would be marginal along with the advent of large-scale on-chip silicon photonics (SiP) integration technologies. Furthermore, the unique advantage of

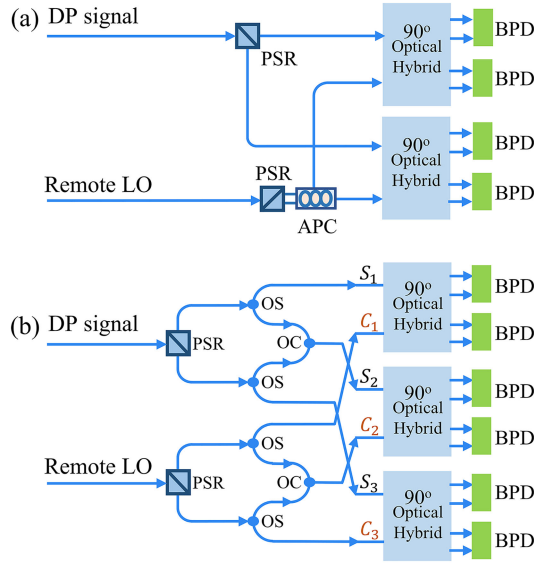


Fig. 1. Configuration of (a) conventional PDCR using an APC for remote LO and (b) proposed C-PDCR without any optical polarization control for remote LO. DP: dual-polarization. PSR: polarization splitter/rotator. OC/OS: optical coupler/splitter. BPD: balanced photodetector.

the proposed C-PDCR is that the polarization fading issue is fully addressed without any optical polarization control by the complementary polarization detection and electronic DSP.

In the proposed C-PDCR, the received DP signals and the remotely delivered LO are all first decomposed into two single-polarization signals by using PSRs similar to the conventional PDCR. The two branches of either the DP signal or the remote LO after the PSRs are optically combined using optical splitters/couplers only to obtain complementary polarization output. Together with the complementary polarization output, the three optical polarization signals from the DP signals are mixed with the three corresponding optical outputs from the remote LO through three 90-degree optical hybrids. The electrical fields of the received DP signal S and remote LO C are denoted as

$$S = [S_X, S_Y] \quad (1)$$

$$C = [C_X, C_Y] \left(|C_X|^2 + |C_Y|^2 \neq 0 \right) \quad (2)$$

where X/Y is the electrical field of two orthogonal polarizations. To avoid the polarization fading, the manual intervention method of using APC is necessitated for the conventional PDCR. Ignoring some trivial constants and phase delays for explanation simplicity, the enhanced polarization signal S_E and LO C_E fed into the three 90-degree optical hybrids are expressed as

$$S_E = [S_1, S_2, S_3] = \left[S_X, (S_X + S_Y)/\sqrt{2}, S_Y \right] \quad (3)$$

$$C_E = [C_1, C_2, C_3] = \left[C_X, (C_X + C_Y)/\sqrt{2}, C_Y \right] \quad (4)$$

where S_2/C_2 are the complementary polarization optical signals. Therefore, it can be inferred that the vector S_E and C_E all have three components but only with the dimensionality of two. To avoid the complicated APC used in conventional PDCR,

the redundant polarization component, namely complementary polarization optical signals in the proposed C-PDCR are indispensable for remote LO C to be an enhanced remote LO C_E . Similar to the conventional PDCR, one polarization tributary C_1/C_3 would be zero due to the nature of single-polarization LO when the polarization fading effect occurs. Note that the two polarization tributaries C_1 and C_3 of the remote LO could not be in fading simultaneously due to the constraint $|C_X|^2 + |C_Y|^2 \neq 0$. In this situation, the complementary polarization tributary C_2 could regenerate the faded polarization tributary. This enables the resilient reconstruction of the received remote LO even when the received remote LO fades along with one of the polarization axes. However, when there is no polarization fading, the two polarization tributaries C_1 and C_3 would have the same power but with the phase difference of π , which results in fading of the complementary polarization signal C_2 . Under such circumstances, the two polarization tributaries C_1 and C_3 preserve the LO power and provide polarization-diversity detection, which functions as the conventional PDCR. Consequently, our proposed C-PDCR scheme is fundamentally resilient against arbitrary SOP of the received remote LO. From the three 90-degree optical hybrids followed by BPDs, the obtained electrical output R_E after complex signal forming is given by

$$R_E = S_E \circ C_E^* = [S_1 C_1^*, S_2 C_2^*, S_3 C_3^*] \quad (5)$$

where the operator ' \circ ' denotes element-wise product and ' $*$ ' represents for complex conjugate. The obtained electrical output R_E is a linearized field vector and contains a linear combination of the transmitted DP signals. To perform polarization demultiplexing, namely, polarization tracking, the 3×2 MIMO in Jones space [18]–[19] could be deployed to retrieve the transmitted DP signals. Compared with the standard DSP utilized as a benchmark for the conventional PDCR, the only small modification is the polarization demultiplexing algorithm or the MIMO and most of the legacy coherent DSP stack is reusable.

III. EXPERIMENTAL SETUP

To validate our proposed C-PDCR scheme in a proof-of-concept experiment, a 1.08-Tb/s DP transmission experiment is carried out with the experimental setup presented in Fig. 2. As discussed before, self-coherent homodyne detection significantly relaxes the requirements on the laser sources and allows for employing distributed feedback (DFB) lasers when the optical paths of the DP signal and the remote LO are strictly aligned up. For the proof-of-concept demonstration, the laser source with 15-kHz linewidth is employed for the generation of both DP signals and self-coherent remote LO. To avoid complicated physical length matching, multi-core fiber would be a good option when using low-cost lasers with large linewidth. Moreover, the received remote LO could be optically amplified to be shared among multiple cores for self-coherent homodyne detection. A 90-Gbaud single-polarization OFDM signal is first generated with a 100-GSa/s sampling rate. The discrete Fourier transform (DFT) size is 4096, in which 3687 subcarriers are filled with probabilistic constellation shaped (PCS) 256-QAM symbols. Typically, the modulation formats are operated at a capacity

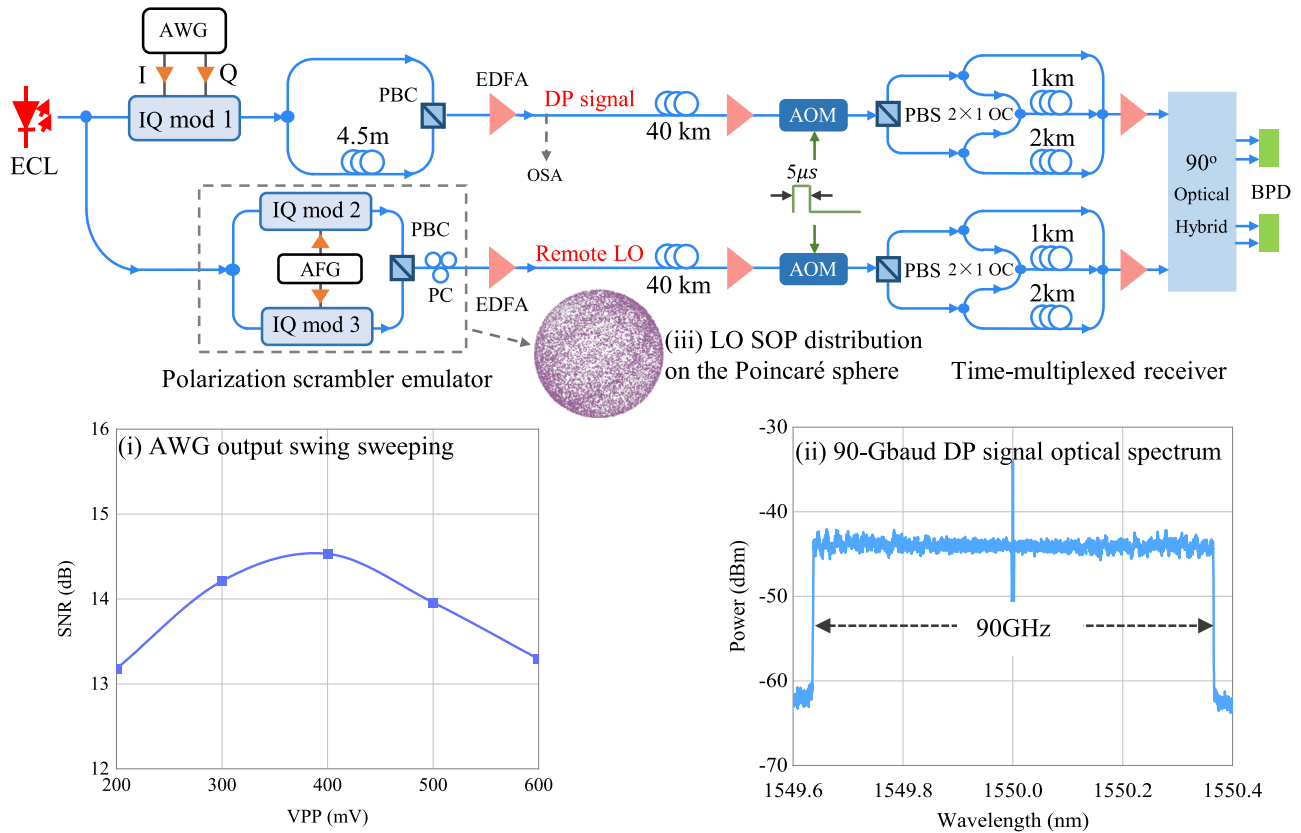


Fig. 2. Experimental setup. ECL: external cavity laser. IQ mod: IQ modulator. AWG/AFG: arbitrary waveform/function generator. PC: polarization controller. PBS/PBC: polarization beam splitter/combiner. OSA: optical spectrum analyzer. AOM: acoustic-optic modulator. OC: optical coupler. Insets (i-iii) are labeled with titles in the figure, respectively.

close to the Shannon limit e.g., 15% to 25% below its maximum [20]. Therefore, the constant composition distribution matcher (CCDM) is deployed to yield the PCS-256QAM symbols with an entropy of 6 bits/symbol. As the CD is post compensated, the cyclic prefix (CP) for the OFDM signal is not added to the signal sequence. To compensate for the low-pass characteristic of the used IQ modulator and realize uniform entropy loading among subcarriers, the electrical pre-emphasis in the frequency domain is implemented. Before loading the data to the arbitrary waveform generator (AWG), the field signals are clipped to suppress the peak-to-average-power ratio (PAPR) for fully utilizing the quantization bits of the AWG. The output swing of AWG is swept for finding the optimal operation point (OP) to linearly drive the IQ modulator and maximize the output power of the IQ modulator simultaneously. The parametric study of the AWG output swing is presented in inset (i) of Fig. 2. Hence, the optimal OP of AWG output swing is 400 mV for this experiment. The DP signal is produced by the optical polarization emulator, in which a 4.5-m optical delay line is used for signal decorrelation. The optical delay for decorrelation is much longer than the equivalent time delay of the accumulated fiber CD and the subsequent least mean square (LMS) algorithm. The optical spectrum of the generated DP signal with 90-GHz optical bandwidth is shown in inset (ii) of Fig. 2.

To evaluate this polarization-diversity self-coherent homodyne detection system, polarization scrambling is an essential

procedure. For this purpose, a polarization scrambler [21] is assembled by using the discrete components, which are shown in the dashed box of Fig. 2. It consists of two low-speed IQ modulators and a manually tuned polarization controller (PC). In the emulated polarization scrambler, the two IQ modulators are driven by two radio signals $\cos(2\pi ft)$ and $\sin(2\pi ft)$, respectively, where f is polarization rotation frequency in the Jones space. Driven by these two radio signals only, the trajectory of the SOP of remote LO will be a circle with a state transition frequency of $2f$ due to the second-order representation of Stokes parameters [22]–[23]. For the sake of traversing all the SOP on the Poincaré sphere, the manually tuned PC is put to use and the transmission fiber with distributed time-varying birefringence could also offer randomness. The depolarized SOP distribution of the remote LO on the Poincaré sphere is simulated and illustrated in inset (iii), which verifies the effectiveness of our assembled emulator of polarization scrambler. The DP signal and the depolarized remote LO are launched into a pair of 40-km fibers.

At the receiver side, a time-multiplexed receiver configuration using acoustic-optic modulators (AOMs) is implemented to save the number of needed analog-to-digital converters (ADCs) and BPDs (this configuration is not needed in a field receiver). The two AOMs are utilized to perform the gate function with 15- μ s period and 33.33% duty cycle. The three polarization optical signals from either DP signal or remote LO in the C-PDCR

configuration are delayed by 0, 1, 2-km optical delay lines, respectively, for achieving strict time separation. The three delayed optical signals from either DP signal or remote LO are optically combined by using 3×1 optical couplers and then optically amplified by EDFAs to compensate for the lossy receiver configuration. The optically amplified DP signals and the remote LO are fed into the 90-degree optical hybrid for coherent detection. Note that the excessive number of EDFA used in this experiment is just for lab demonstration. In practice, there are no EDFAs needed for cost-sensitive short-reach applications. The received electrical signals from the two BPDs are sampled by a 160-Gsa/s oscilloscope. In the receiver-side DSP, the carried-out steps are (i) resampling to 2 samples/symbol; (ii) accumulated CD compensation; (iii) frame synchronization; (iv) real-valued T/2-spaced 6×4 MIMO based on normalized LMS (NLMS) algorithm [24] for polarization tracking and demultiplexing in the time domain; (v) channel equalization; (vi) carrier phase recovery; (vii) mutual information calculation. As the real-valued MIMO is utilized, part of the transmitter-side and receiver-side IQ/polarization imbalance could be compensated. The convergence time for the NLMS-based MIMO is around 12.5 ns in this experiment for both back-to-back (BtB) and 40-km fiber transmission cases, which is sufficient for tracking 80-Mrad/s polarization rotation. For performance evaluation, generalized mutual information (GMI) [25] is calculated under bit-metric decoding (BMD). GMI is the maximum amount of information that can be transmitted with a negligible error rate under BMD. To reliably quantify the post-FEC performance, normalized GMI (NGMI) [26] is utilized as it quantifies the maximum information per transmitted bit having the same implication as to the FEC code rate. NGMI is a modulation format-agnostic figure of merit for soft-decision forward error correction (SD-FEC) [26].

IV. RESULTS AND DISCUSSIONS

A. Parametric Study of LOSPR for the Proposed C-PDCR

To maximize the system efficiency, the LOSPR is investigated. We control the optical power of the DP signal and the remote LO fed into the 90-degree optical hybrid. The LOSPR is swept for both BtB and 40-km fiber transmission. The result is presented in Fig. 3. At 5-dB LOSPR, the SNR performance achieves the highest. However, after 40-km fiber transmission, the LOSPR performance is all below the BtB. The accumulated fiber CD could be compensated by the advanced DSP. The performance difference could be attributed to the optical noise-contaminated LO by the EDFAs at the receiver side, which is necessitated for the lossy time-multiplexed receiver configuration. Benefiting from the EDFAs at the receiver side, our system could be handled at the high-power level to get the strong electrical outputs from BPDs. Therefore, the power of the beating term between the signal and LO could be maximized at the lower LOSPR. In practice, the received DP signal power could be lower without the EDFA. Higher LOSPR could be required to enhance the beating power of the DP signal and remote LO.

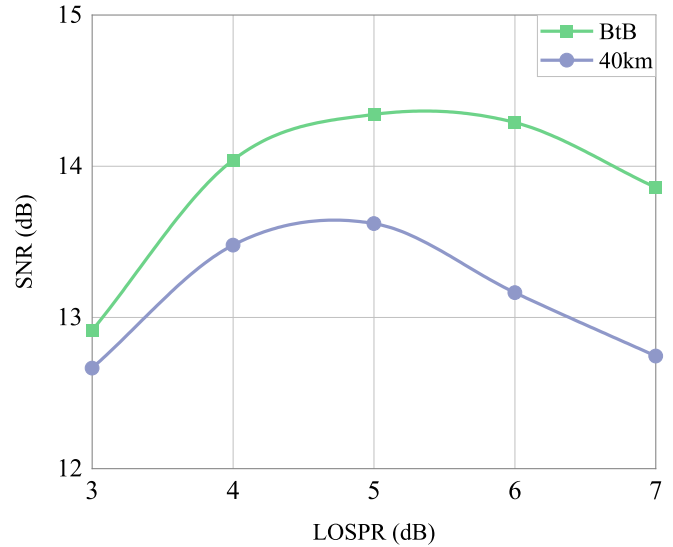


Fig. 3. Achieved SNR under different LOSPR at back-to-back (BtB) and 40-km fiber transmission.

B. Polarization Tracking Capability of the Proposed C-PDCR

To reveal the effectiveness of our proposed C-PDCR scheme using remote LO for combating the polarization fading issue, we select a special SOP (where the polarization scrambler is turned off) when the received electrical waveforms from a pair of BPDs have power fading, namely, polarization fading. The real-valued 6×4 MIMO could retrieve the transmitted DP signal. The electrical spectrum comparison before/after the MIMO is made as shown in Fig. 4(a). The filter gain of the MIMO is normalized to guarantee the same input and output power. As illustrated in Fig. 4(a), the power density of one MIMO input approaches the noise floor while the other two inputs have a strong power density. As analyzed in Section II, the MIMO has at least two strong inputs even in the situation of polarization fading. By the real-valued 6×4 MIMO for polarization demultiplexing and tracking, the transmitted DP field signal is successfully retrieved with the same power density for the recovered DP electrical spectrums.

To signify the robustness of the proposed C-PDCR scheme against the fast SOP variations of the remote LO, the GMI performance is evaluated under different SOP rotation rates of remote LO. The results of fast polarization tracking capability are presented in Fig. 4(b) for BtB and 40-km transmission. The GMI performance is quite stable with negligible fluctuations under the LO SOP rotation rate up to 314 krad/s in this experiment. This represents a 1047-fold or more than 3-order improvement of the polarization tracking speed compared to the prior report [15]. This also signifies a great advantage of our proposed C-PDCR over conventional PDCR.

C. Transmission Performance

The OSNR performance of the proposed C-PDCR scheme with a 1.08-Tb/s raw data rate is presented in Fig. 5. The GMI performance as a function OSNR is depicted in Fig. 5(a) for

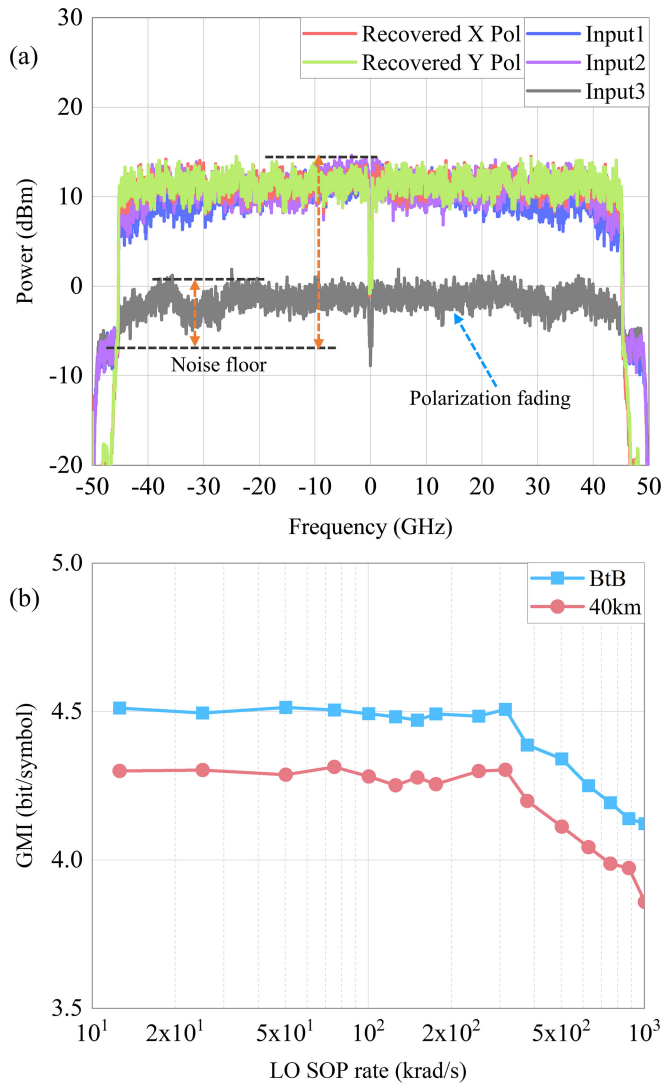


Fig. 4. (a) Electrical spectra before/after MIMO when polarization fading occurs. (b) GMI as a function of LO SOP rotation speed at the OSNR of 25 dB. BtB: back-to-back.

BtB and 40-km fiber transmission where the theoretical GMI performance is obtained by numerical simulation with the same transmitter DSP. The recovered PCS-256QAM before/after the fiber transmission is shown in the insets (i-ii) with a circular symmetric complex Gaussian distribution [27]. The DP constellations are incorporated into the plot. Fig. 5(b) illustrates the NGMI performance for predicting the post-FEC performance. We take a practical NGMI threshold of 0.8 using 27.5% SD-FEC overhead [28]. When the system reaches the NGMI threshold, error-free transmission could be claimed by a practical FEC. The OSNR sensitivity for back-to-back (BtB) and 40-km transmission is 24 dB and 25 dB, respectively. The 1-dB OSNR sensitivity difference could be attributed to the increased noise power in the received LO added by the optical amplifiers as aforementioned. Moreover, the transmitter IQ imbalance-induced performance degradation could be further aggravated by the fiber chromatic dispersion. Compared with the theoretical NGMI performance,

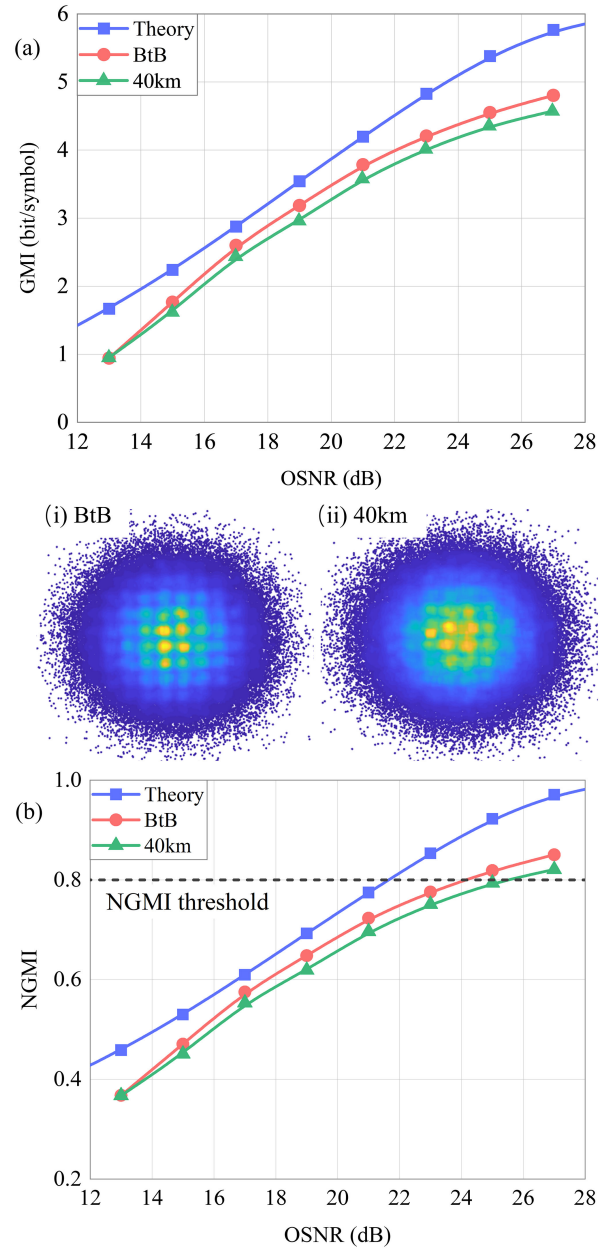


Fig. 5. GMI (a) and NGMI (b) performance as a function of OSNR for the proposed C-PDCR scheme with 1.08-Tb/s data rate. Insets (i-ii): recovered PCS-256QAM constellations at 27-dB OSNR.

the OSNR sensitivity gap is approximately 3-4 dB. It can be seen that there is a strong unsuppressed optical carrier in the optical spectrum of the inset (ii) of Fig. 2. Moreover, the time-multiplexed receiver configuration for demonstrating the proposed C-PDCR scheme is quite lossy and noisy, and the transmitter in this experiment has been pushed to its limit. All of these reasons result in the large OSNR sensitivity difference. Fig. 6 shows the recovered SNR of each subcarrier for the OFDM-modulated DP signal. Both polarizations have a similar recovered SNR. It is observed that some subcarriers are greatly degraded due to the clock leakage from the 100-GSa/s AWG.

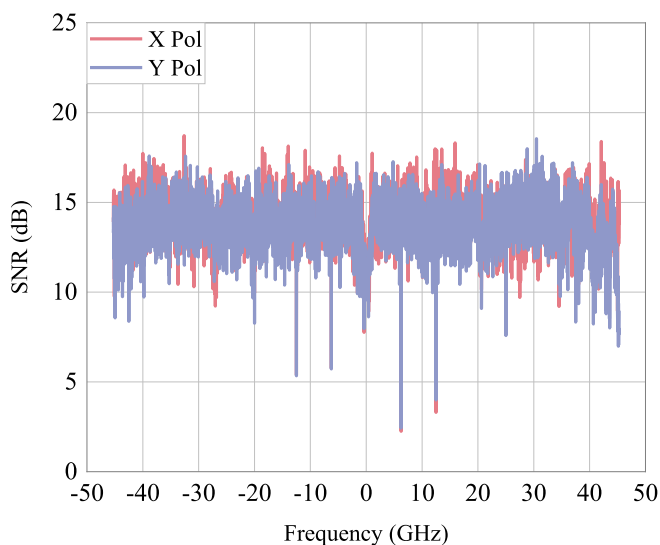


Fig. 6. Recovered SNR of each subcarrier for two polarizations after 40-km transmission at 27-dB OSNR. X/Y Pol: X/Y polarization.

Excluding the FEC overhead by discriminating the shaping factor in the probabilistic amplitude shaping (PAS) structure [29], the achieved net data rate is 769.4 Gb/s over 45-GHz electrical bandwidth in this experiment.

V. CONCLUSION

In this paper, we have proposed and demonstrated a C-PDCR scheme based on complementary polarization detection using three 90-degree optical hybrids for self-coherent homodyne detection. The proposed C-PDCR could utilize the remotely delivered LO without optical polarization control and is fundamentally robust against any input SOP of the receiver remote LO. The robustness of the proposed C-PDCR is verified and demonstrated by a proof-of-concept experiment with a 1.08-Tb/s line rate (net rate 769.4 Gb/s over 45-GHz electrical bandwidth). The polarization tracking speed of the proposed C-PDCR leveraging the normal MIMO algorithm could reach up to 314-krad/s SOP rotation rate of remote LO without GMI performance degradation, which represents more than 3-order of magnitude improvements compared with the prior reports. Therefore, the proposed C-PDCR scheme could be a good solution for future 800G/1.6T Ethernet interface speeds.

REFERENCES

[1] Cisco Global Cloud Index 2015-2020. San Jose, CA, USA: Cisco Corp., Nov. 2016.
 [2] 2018 Ethernet Roadmap, [Online]. Available: <http://ethernetalliance.org/the-2018-ethernetroadmap/>
 [3] X. Zhou, R. Urata, and H. Liu, "Beyond 1 Tb/s intra-data center interconnect technology: IM-DD OR coherent?," *J. Lightw. Technol.*, vol. 38, no. 2, pp. 475–484, Jan. 2020.
 [4] [Online]. Available: http://www.ieee802.org/3/bs/public/15_03/index.shtml
 [5] R. Nagarajan, M. Filer, Y. Fu, M. Kato, T. Rope, and J. Stewart, "Silicon photonics-based 100 Gbit/s, PAM4, DWDM data center interconnects," *IEEE/OSA J. Opt. Commun. Netw.*, vol. 10, no. 7, pp. 25–36, Jul. 2018.

[6] D. Che et al., "Single-channel direct detection reception beyond 1 Tb/s," in *Proc. Opt. Fiber Commun. Conf. Postdeadline Papers*, 2019, pp. 1–3.
 [7] K. Kikuchi and S. Kawakami, "Multi-level signaling in the stokes space and its application to large-capacity optical communications," *Opt. Exp.*, vol. 22, no. 7, pp. 7374–7387, 2014.
 [8] P. Dong, X. Chen, K. Kim, S. Chandrasekhar, Y.-K. Chen, and J. H. Sinsky, "128-Gb/s 100-km transmission with direct detection using silicon photonic stokes vector receiver and I/Q modulator," *Opt. Exp.*, vol. 24, no. 13, pp. 14208–14214, 2016.
 [9] C. Doerr et al., "Single-chip silicon photonics 100-Gb/s coherent transceiver," in *Proc. Opt. Fiber Commun. Conf.*, 2014, Paper Th5C.1.
 [10] T. Hayashi et al., "125- μ m-cladding eight-core multi-core fiber realizing ultra-high-density cable suitable for O-Band short-reach optical interconnects," *J. Lightw. Technol.*, vol. 34, no. 1, pp. 85–92, 2016.
 [11] M. Morsy-Osman et al., "DSPfree 'coherent-lite' transceiver for next generation single wavelength optical intra-datacenter interconnects," *Opt. Exp.*, vol. 26, no. 7, pp. 8890–8903, 2018.
 [12] C. K. Madsen et al., "Reset-free integrated polarization controller using phase shifters," *IEEE J. Sel. Topics Quantum Electron.*, vol. 11, no. 2, pp. 431–438, Mar./Apr. 2005.
 [13] Q. Hu, X. Chen, A. Li, and W. Shieh, "High-dimensional stokes-space analysis for monitoring fast change of mode dispersion in few-mode fibers," in *Proc. Opt. Fiber Commun. Conf.*, 2014, pp. 1–3.
 [14] D. Charlton et al., "Field measurements of SOP transients in OPGW, with time and location correlation to lightning strikes," *Opt. Exp.*, vol. 25, pp. 9689–9696, 2017.
 [15] T. Gui, X. Wang, M. Tang, Y. Yu, Y. Lu, and L. Li, "Real-time demonstration of 600 Gb/s DP-64QAM selfhomodyne coherent bi-direction transmission with uncooled DFB laser," in *Proc. Opt. Fiber Commun. Conf.*, 2020, Paper Th4C.3.
 [16] H. Ji, X. Zhou, C. Sun, and W. Shieh, "Polarization-diversity receiver using remotely delivered local oscillator without optical polarization control," *Opt. Exp.*, vol. 28, pp. 22882–22890, 2020.
 [17] H. Ji et al., "Complementary polarization-diversity self-coherent homodyne receiver with rapid polarization tracking," in *Proc. Opt. Fiber Commun. Conf.*, 2022, pp. 12878–12890.
 [18] S. J. Savory, "Digital coherent optical receivers: Algorithms and sub-systems," *IEEE J. Sel. Topics Quantum Electron.*, vol. 16, no. 5, pp. 1164–1179, Sep./Oct. 2010.
 [19] E. Ip, A. P. T. Lau, D. J. F. Barros, and J. M. Kahn, "Coherent detection in optical fiber systems," *Opt. Exp.*, vol. 16, no. 2, pp. 753–791, 2008.
 [20] F. Buchali et al., "DCI field trial demonstrating 1.3-Tb/s single-channel and 50.8-Tb/s WDM transmission capacity," *J. Lightw. Technol.*, vol. 38, pp. 2710–2718, 2020.
 [21] F. Heismann and R. W. Smith, "High-speed polarization scrambler with adjustable phase chirp," *IEEE J. Sel. Topics Quantum Electron.*, vol. 2, no. 2, pp. 311–318, Jun. 1996.
 [22] D. Che, A. Li, X. Chen, Q. Hu, Y. Wang, and W. Shieh, "160-Gb/s stokes vector direct detection for short reach optical communication," in *Proc. Opt. Fiber Commun. Conf.*, 2014, pp. 1–3.
 [23] G. Milione, H. I. Sztul, D. A. Nolan, and R. R. Alfano, "Higher-order poincaré sphere, stokes parameters, and the angular momentum of light," *Phys. Rev. Lett.*, vol. 107, no. 5, 2011, Art. no. 053601.
 [24] D. T. M. Slock, "On the convergence behavior of the LMS and the normalized LMS algorithms," *IEEE Trans. Signal Process.*, vol. 41, no. 9, pp. 2811–2825, Sep. 1993.
 [25] A. Alvarado, E. Agrell, D. Lavery, R. Maher, and P. Bayvel, "Replacing the soft-decision FEC limit paradigm in the design of optical communication systems," *J. Lightw. Technol.*, vol. 34, no. 2, pp. 707–721, Jan. 2016.
 [26] J. Cho, L. Schmalen, and P. J. Winzer, "Normalized generalized mutual information as a forward error correction threshold for probabilistically shaped QAM," in *Proc. Eur. Conf. Opt. Commun.*, 2017, pp. 1–3.
 [27] F. Buchali, F. Steiner, G. Böcherer, L. Schmalen, P. Schulte, and W. Idler, "Rate adaptation and reach increase by probabilistically shaped 64-QAM: An experimental demonstration," *J. Lightw. Technol.*, vol. 34, no. 7, pp. 1599–1609, 2016.
 [28] R. Maher, K. Croussore, M. Lauer mann, R. Going, X. Xu, and J. Rahn, "Constellation shaped 66 GbD DP-1024QAM transceiver with 400 km transmission over standard SMF," in *Proc. Eur. Conf. Opt. Commun.*, 2017, pp. 1–3.
 [29] X. Chen, G. Raybon, D. Che, J. Cho, and K. W. Kim, "Transmission of 200-Gbaud PDM probabilistically shaped 64-QAM signals modulated via a 100-GHz Thin-film LiNbO₃ I/Q modulator," in *Proc. Opt. Fiber Commun. Conf.*, 2021, pp. 1–3.